JOURNAL OF COMPUTATIONAL PHYSICS 38, 237–250 (1980)

A Magnetohydrodynamic Particle Code with Force Free Electrons for Fluid Simulations

T. TAJIMA, J. N. LEBOEUF, AND J. M. DAWSON

Department of Physics, University of California, Los Angeles, California 90024

Received April 10, 1979; revised November 9, 1979

The two-fluid dynamics of plasmas with force free electrons under the quasi-neutral condition can be described by the one-fluid magnetohydrodynamic equations with addition of a single term, the Hall term, to the field induction equation. This algorithm is implemented in a magnetohydrodynamic particle code to represent some aspects of electron–ion plasmas in the Lagrangian framework with a fixed uniform background grid. The code sustains, for example, Alfven-ion cyclotron waves and whistler waves, as is demonstrated by the dispersion, polarization and propagation of these waves.

I. INTRODUCTION

The study of slow-time-scale phenomena in plasma physics compared with the plasma or gyro periods, such as magnetohydrodynamic stability, drift waves, diffusion and energy transport, is essential to fusion plasma physics among other disciplines. It is, therefore, of importance to generate numerical algorithms which can accommodate simulations of such phenomena. To investigate these slow processes via computer simulation within reasonable accuracy and practical means requires techniques which dispense with high-frequency phenomena without compromising the validity of the physics at lower frequencies.

One recent approach to achieve this goal has been to introduce quasi-neutrality in finite-size particle codes of electrostatic or magnetostatic denominations. Okuda *et al.* [1] eliminated the high-frequency space charge oscillations from an electrostatic code by having the adiabatic electrons follow the ion density fluctuations, unmodified in the process, so as to represent Debye shielding and preserve quasi-neutrality. This approach may be called a renormalization method. On the magnetostatic front, Hewett and Nielson [2] have constructed a quasi-neutral hybrid model, where the ions are represented by the usual particle-in-cell technique. The electrons, however, are considered to be a neutralizing thermal fluid retaining some inertial properties. The fields are calculated in the nonradiative Darwin limit, and the electrostatic field is obtained by solving the quasi-neutral Poisson equation. Byers *et al.* [3] have developed an algorithm where Maxwell's equations are also solved in the limits of the magnetostatic approximation and quasi-neutrality. This model treats electrons as a

0021-9991/80/140237–14$02.00/0

581/38/2-9

massless fluid and ions as particles and examines phenomena at frequencies lower than the lower hybrid frequency where electron inertia can be neglected altogether.

The other well-established approach in keeping with lengthening the time step as much as possible and simulating long-time-scale phenomena has been to solve for the plasma evolution in the magnetohydrodynamics approximation [4]. The one-fluid codes most commonly used do not make any distinction between electrons and ions and treat the plasma through its mass density, fluid density and current density. So doing, one can automatically dispense with such fast-time-scale phenomena as electron plasma oscillations and gyro oscillations; at the same time, one loses most of the electron physics. Resorting to a two-fluid code entails pushing the electrons on the time scale of the plasma or gyro frequency and goes against the purpose of lengthening the time step.

We present here an algorithm which is a simple modification of the recently developed magnetohydrodynamics code [5], where elements of the fluid are represented by finite-size particles. To enrich the physics involved, it is essential to treat the electron dynamics and avoid pushing on the fast electron time scale. The adoption of a force free electron dynamics algorithm introduces a Hall term in the magnetic field updating equation. The addition of the Hall term means that the particles now represent an ion fluid. With this code, Alfven-ion cyclotron waves and whistler waves, for example, are incorporated.

The organization of the paper is as follows. A description of the algorithm is given in Section II. Section III is devoted to tests of the model with respect to dispersion relation, propagation and polarization diagnostics, while the final section draws conclusions.

II. Algorithm for Quasi-neutral Magnetohydrodynamics with Force Free Electrons

To facilitate the description of our model for the electron–ion magnetohydrodynamic particle code, let us briefly review the algorithm of the one-fluid magnetohydrodynamic particle code [5]. In this code, the particle quantities, such as position and momentum, are pushed in a Lagrangian way, while the magnetic fields are advanced in an Eulerian manner. The position of a particle is found by $d\mathbf{r}_j(t)/dt = \mathbf{v}_j(t)$. In the ideal one-fluid MHD description of a plasma, the equation of motion for each "particle" is

$$d\mathbf{v}_j(t)/dt = -(1/\rho)\,\nabla P - (1/8\pi\rho)\,\nabla B^2 + (1/4\pi\rho)\nabla \cdot (\mathbf{BB}), \tag{1}$$

where ρ is the mass density of the fluid averaged over electrons and ions. The left-hand side of Eq. (1) is the total derivative of the jth particle velocity while the right-hand side only involves macroscopic quantities defined at the mesh points of the fixed background grid. The density and velocity of the fluid are given by nearest grid point interpolation of the respective particle quantities in a cell, i.e.,

$$n_g(\mathbf{r}) = \sum_{j \in g} f(\mathbf{r} - \mathbf{r}_j), \tag{2}$$

$$\mathbf{v}_g(\mathbf{r}) = \sum_{j \in g} \mathbf{v}_j / \sum_{j \in g} 1. \tag{3}$$

The quantities n_g and v_g are the fluid density and velocity and $f(\mathbf{r} - \mathbf{r}_j)$ is the form factor of the particle, typically a Gaussian one, while the denominator on the right-hand side of Eq. (3) is the number of particles in a cell. The magnetic fields are updated at the mesh points using the fluid velocity:

$$\partial \mathbf{B}/\partial t = \nabla \times (\mathbf{v}_g \times \mathbf{B}). \tag{4}$$

The integration in time of Eq. (4) is carried out by using the conservative Lax method with a time step close to the stability limit so as to avoid excessive numerical diffusion [6].

This ideal magnetohydrodynamic algorithm has dispensed with any distinction between electrons and ions. All the physics is treated through the mass density of the fluid $\rho = (mn_e + Mn_i)/(M + m)$, its flow velocity $v = (mv_e + M\mathbf{v}_i)/(m + M)$, and the current density $\mathbf{J} = -en_e \mathbf{v}_e + en_i \mathbf{v}_i$. To enrich the physics involved, it is essential to treat the electron dynamics. To avoid integrating on the fast electron time scale, we neglect the electron acceleration term which is proportional to the electron mass: the electrons are so light that they instantaneously adjust their velocities to the value determined by the equation of electron motion given by

$$e\left(\mathbf{E} + \frac{\mathbf{v}_e}{c} \times \mathbf{B}\right) - mv_{ei}(\mathbf{v}_i - \mathbf{v}_e) + \frac{1}{n_e} \nabla \cdot \mathbf{P}_e = 0, \tag{5}$$

where v_{ei} is the electron–ion collision frequency, n_e the electron density and $\mathbf{P}_e$ the electron pressure tensor. On the other hand, the equation of motion for ions may be written as

$$M \frac{d\mathbf{v}_i}{dt} = \left(e\mathbf{E} + e \frac{\mathbf{v}_i}{c} \times \mathbf{B}\right) - \frac{1}{n_i} \nabla \cdot \mathbf{P}_i - Mv_{ie}(\mathbf{v}_i - \mathbf{v}_e), \tag{6}$$

where M is the ion mass, $\mathbf{v}_i$ the ion velocity, n_i ($\equiv n$) the ion density and $\mathbf{P}_i$ the ion pressure tensor. Substituting Eq. (5) into the electric field of Eq. (6), we obtain

$$nM \frac{d\mathbf{v}_i}{dt} = \frac{e}{c} n(\mathbf{v}_i - \mathbf{v}_e) \times \mathbf{B} - \nabla \cdot \left(\mathbf{P}_i + \frac{n}{n_e} \mathbf{P}_e\right), \tag{7}$$

Assuming quasi-neutrality ($n_e \cong n_i \equiv n$), therefore, $\mathbf{J} \cong ne(\mathbf{v}_i - \mathbf{v}_e)$, and neglecting the displacement current in Maxwell's equation, we derive the equation of motion for ions as

$$\rho \frac{d\mathbf{v}_i}{dt} = -\frac{1}{4\pi} \mathbf{B} \times (\nabla \times \mathbf{B}) - \nabla \cdot (\mathbf{P}_i + \mathbf{P}_e), \tag{8}$$

where ρ is now the ion mass density. To advance the magnetic field, Faraday's law with Eq. (5) is employed to give

$$\frac{\partial B}{\partial t} = c\nabla \times \left[\frac{\mathbf{v}_i}{c} \times \mathbf{B} + \frac{1}{4\pi ne} \mathbf{B} \times (\nabla \times \mathbf{B}) - \frac{mc\nu_{ei}}{4\pi ne^2} \nabla \times \mathbf{B} + \frac{1}{ne} \nabla \cdot \mathbf{P}_e \right]. \quad (9)$$

Equations (8) and (9) constitute the bases for our model. The second term on the right-hand side of Eq. (9) is just the Hall term. This term has originated from consideration of the electron dynamics through Eq. (5). The velocity $\mathbf{v}_i$ appearing in Eq. (8) is taken to be the ion fluid velocity as per Eq. (3). If the plasma is collisionless ($\nu_{ei} = 0$), the third term on the right-hand side of Eq. (6) and the third term on the right-hand side of Eq. (9) drop out. As was the case with the one-fluid magnetohydrodynamic algorithm, closure of the chain equations of velocity moments is accomplished if one assumes a certain relation of the pressure term to, say, the density. In the present case, on top of such an assumption, a relation between $\mathbf{P}_e$ and $\mathbf{P}_i$ has to be assumed and instituted. Then, the only new term added in Eqs. (8) and (9) is the Hall term in Eq. (9) in comparison with the one-fluid scheme. The current need not be calculated and the algorithm involves essentially the same steps as the one-fluid (ideal) magnetohydrodynamic scheme. The difference between the present algorithm and the quasi-neutral magnetostatic particle algorithm of Byers *et al.* [3] is that this code is faster and dispenses with the ion velocity space information, since this is a fluid code; further, no matrix inversion is required in our code for the ion velocity integration.

III. Tests of the Model

The algorithm described in Section II has been implemented and tested numerically and physically. Physical tests include simulation runs on the code of a thermal plasma as well as of a plasma with launched waves. We check the dispersion relations of the waves obtained from the thermal simulation runs against the theoretical dispersion relation. As a second category of check, phase diagnostics on a particular Fourier component of the fields obtained from simulation runs with launched waves are performed and analyzed in light of the theoretical predictions. The phase diagnostics can determine the propagation direction and polarization as well as the frequency of the waves.

Dispersion Relation

Let us analyze the linear dispersion relation sustained by Eqs. (8) and (9). Neglecting terms involving collisions and pressure for simplicity, we linearize and Fourier transform Eqs. (8) and (9) to obtain

$$-i\omega\, \delta\mathbf{B} = i\mathbf{k} \times (\mathbf{v} \times \mathbf{B}_0) + \alpha \mathbf{k} \times [(\mathbf{k} \times \delta\mathbf{B}) \times \mathbf{B}_0], \quad (10)$$

$$-i\omega\mathbf{v} = (1/\rho)[i(\mathbf{k} \times \delta\mathbf{B}) \times \mathbf{B}_0], \quad (11)$$

where $\alpha \equiv c/4\pi en$, $\delta\mathbf{B}$ and $\mathbf{v}$ represent respectively the perturbed magnetic field and ion fluid velocities, while $\mathbf{B}_0$ stands for the external zeroth order magnetic field. For modes with wavenumber parallel to $\mathbf{B}_0$, which correspond to linearly polarized Alfven waves in ideal magnetohydrodynamics, we obtain, from Eqs. (10) and (11),

$$(\omega^2 - k^2 v_A^2)\,\delta\mathbf{B} - i\alpha\omega(\mathbf{k}\cdot\mathbf{B}_0)(\mathbf{k}\times\delta\mathbf{B}) = 0, \tag{12}$$

with the Alfven speed $v_A = B_0/(4\pi nM)^{1/2}$. Equation (12) yields a dispersion relation

$$\omega = \pm\,[(k^2 v_A^2/2\Omega_i) \pm k v_A(1 + k^2 v_A^2/4\Omega_i^2)^{1/2}], \tag{13}$$

where $\Omega_i \equiv eB_0/Mc$ and $\alpha B_0 = v_A^2/\Omega_i$. The $+$ $(-)$ sign in front of the square bracket in Eq. (13) indicates the forward (backward) propagation and the $+$ $(-)$ sign in front of the second term in the square bracket in Eq. (13) corresponds to the right (left) polarization mode. In the small wavenumber limit ($kv_A/\Omega_i \ll 1$), Eq. (13) becomes

$$\omega \cong k v_A(1 \pm k v_A/2\Omega_i), \tag{14}$$

when forward propagation is retained. In the other limit of large wavenumber ($kv_A/\Omega_i \gg 1$), Eq. (13) reduces to

$$\omega \cong \Omega_i, \qquad k^2 v_A^2/\Omega_i. \tag{15}$$

The first root is that of the ion cyclotron wave and the second that of the whistler. For modes with wavenumber perpendicular to $\mathbf{B}_0$, the magnetosonic branch is recovered from Eqs. (9) and (10), as the Hall term has no effect in this case.

To verify the dispersion relation, a $2\frac{1}{2}$ D (two spatial and three velocity and field dimensions) version of the code is employed in the simulations. The system size is typically $64\Delta \times 16\Delta$ grids (with Δ the unit grid spacing) with four particles in a cell. The external magnetic field $\mathbf{B}_0$ is along the x-axis and its strength is such that $v_A = 3c_s$, c_s being the sound speed. The parameter α is such that $\Omega_i = 3c_s/\Delta$. Small random velocities ($0.1\,c_s$) are given in all three directions at $t = 0$ (the thermal run). The time step is chosen to $\Delta t = 0.15\,c_s^{-1}\Delta$ throughout; time autocorrelations of the induced magnetic fields in the y and z directions are then taken numerically over the whole extent of the runs, typically $200\,c_s^{-1}\Delta$. The frequencies are obtained from peaks in the power spectral density for each ($k_x \neq 0$, $k_y = 0$) mode.

The simulation dispersion relation is plotted in Fig. 1. The lower solid curve indicates the Alfven-ion cyclotron branch obtained from the theoretical dispersion relation, Eq. (13), while the upper curve follows the theoretical whistler branch. The code reproduces the correct behavior in the long wavelength limit. The whistler (solid dots) and Alfven ion-cyclotron branches (crosses) are clearly separated. The theoretical frequency separation between the two branches in the long wavelength regime is

$$\Delta\omega = k v_A(k v_A/\Omega_i). \tag{16}$$

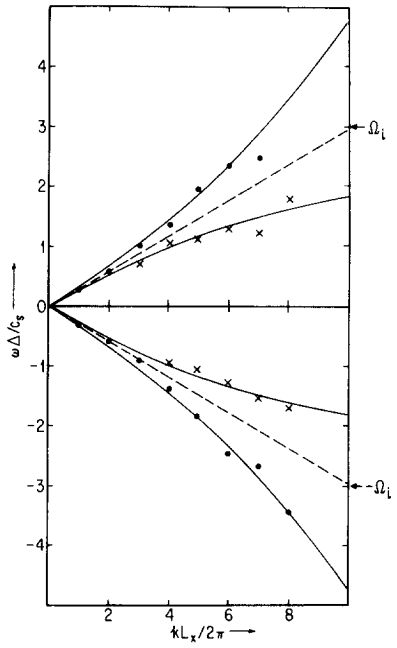

FIG. 1. Dispersion relation. The solid curves are obtained from theory with $v_A = 3.0\, c_s$ and $\Omega_i = 3.0\, c_s \Delta^{-1}$. The dashed lines represent $\omega = kv_A$. The solid dots fall on the whistler branch while the crosses lie on the ion-cyclotron branch.

The simulation value for $\Delta\omega$ is within 5% of that calculated by Eq. (16). As expected, the magnetosonic branch was unaffected by the Hall term in the simulation. In the short wavelength regime, the spectrum intensity peaks in the simulation are less prominent and the obtained frequency values tend to fluctuate and, for the whistler branch in particular, tend to undershoot the theoretical values. This is believed to be due to the finite grid size (see the Appendix).

Polarization and Propagation Diagnostics

The code should not only represent the correct frequencies of the modes described in the above, but also preserve correct relations for various wave phases: for example, the parallel propagating whistler wave is right-circularly polarized and the Alfven-ion cyclotron left-circularly. In the following simulations, we excite, at $t = 0$, either a linearly polarized wave or a left-circularly polarized wave by self-consistently perturbing the perpendicular magnetic fields and the fluid (particle) velocities, and follow the wave propagation. No random velocities associated with the particles are given. For theoretical comparison the ratios of the real to imaginary part of the y component of the magnetic field at the wavelength of the initial perturbation and the ratio of the real parts of the y and z components of the fields are evaluated. Two phase angles obtained from the launched wave simulations, $\theta = \tan^{-1}(\delta B_y^R/\delta B_y^I)$ and

$\theta_R = \tan^{-1}(\delta B_y^R/\delta B_z^R)$, are plotted versus time. The first is a measure of the propagation directions and the second indicates polarizations

For the first case, we give a perturbation at $t = 0$ of the form

$$\delta B_y = \varepsilon B_0 \sin kx,$$
$$\delta v_y = -\varepsilon \left(\frac{kv_A}{\omega}\right) c_s \sin kx, \tag{17}$$

with $k_x = (2\pi/L_x)m$, $m = 2$ and $\varepsilon = 0.02$. This choice of δB_y and δv_y ensures forward propagation of the disturbance. It also favors excitation of both the left and right

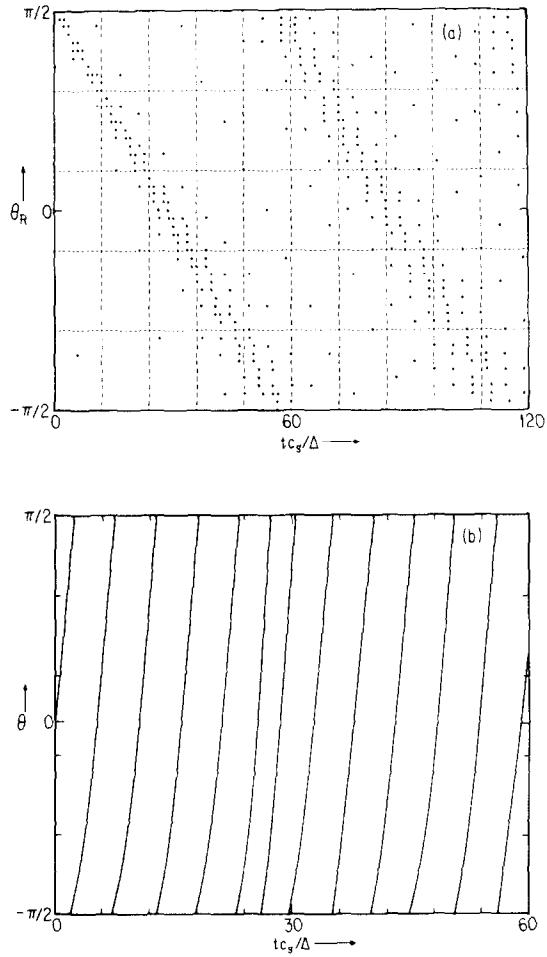

FIG. 2. Phase diagnostics: linearly polarized forward propagating launched wave with wavenumber $k = (2\pi/L_x)m$, $m = 2$. (a) The temporal behavior of the simulation angle $\theta_R = \tan^{-1}(\delta B_y^R/\delta B_z^R)$. (b) The time evolution of the simulation angle $\theta = \tan^{-1}(\delta B_y^R/\delta B_y^I)$.

polarizations, since Eq. (17) does not dictate δB_z and δv_z. Therefore, the perturbation will more likely be the linearly polarized forward propagating wave. Note that the eigenfrequencies of the two polarizations are close to each other for this wavenumber. The simulation results for θ and θ_R are shown in Fig. 2.

Suppose that the perturbation, Eq. (17), induces the same amplitudes for the two polarizations. Then, the temporal behavior of the induced magnetic field oscillations for $t > 0$ are

$$\begin{aligned} \delta B_y &= (\varepsilon/2) B_0[\cos(kx - \omega_- t) + \sin(kx - \omega_+ t)], \\ \delta B_z &= -(\varepsilon/2) B_0[\cos(kx - \omega_- t) - \cos(kx - \omega_+ t)], \end{aligned} \tag{18}$$

where ω_- refers to the Afven-ion cyclotron frequency and ω_+ the whistler frequency. We take a Fourier transform of the quantities in Eq. (18) in space with respect to the wavenumber k and calculate the ratios

$$\begin{aligned} \delta B_y^R / \delta B_y^I &= +\tan \omega_H t, \\ \delta B_y^R / \delta B_z^R &= \cot \omega_L t, \end{aligned} \tag{19}$$

where the superscripts R and I denote the real and imaginary parts of the transformation and $\omega_L = (\omega_+ - \omega_-)/2 = \Delta\omega/2$ and $\omega_H = (\omega_+ + \omega_-)/2$ ($\simeq k v_A$). It follows from Eq. (19) that

$$\begin{aligned} \theta(t) &= \omega_H t, \\ \theta_R(t) &= \pi/2 - \omega_L t \cong \pi/2 - 1/2 k v_A (k v_A/\Omega_i) t. \end{aligned} \tag{20}$$

The angle θ in Eq. (20) is a measure of forward propagation, since θ increases (decreases) as t increases for forward (backward) propagation. Similarly, the appearance of the frequency ω_L in θ_R is an indication of a mix of two polarizations. This is indeed what is observed in Fig. 2a for θ and Fig. 2b for θ_R. Furthermore, the period from Fig. 2a is obtained as $\tau \sim 10\, c_s^{-1}\Delta$ while from Eq. (20) it should be $\tau = 2\pi\omega_H^{-1} \sim 10.7\, c_s^{-1}\Delta$. Also from Fig. 2b, the period is $\tau \sim 120\, c_s^{-1}\Delta$, while from θ_R of Eq. (20) it should be $\tau = 108.7\, c_s^{-1}\Delta$. Appearance of a structure at a shorter period (approximately that of the whistler) in Fig. 2b is due to the slightly unbalanced excitation of the two polarizations.

To excite a left-circularly polarized wave, a run was carried out with the initial perturbations

$$\begin{aligned} \delta B_y &= \varepsilon B_0 \cos kx; \qquad \delta v_y = -\varepsilon(k v_A/\omega) c_s \cos kx, \\ \delta B_z &= \varepsilon B_0 \sin kx; \qquad \delta v_z = -\varepsilon(k v_A/\omega) c_s \sin kx, \end{aligned} \tag{21}$$

with $\varepsilon = 0.02$ and $k = (2\pi/L_x)m$, $m = 2$. This perturbation establishes forward propagation. Such an initial perturbation should propagate the following wave:

$$\begin{aligned} \delta B_y &= \varepsilon B_0 \cos(kx - \omega_- t), \\ \delta B_z &= \varepsilon B_0 \sin(kx - \omega_- t). \end{aligned} \tag{22}$$

Fourier transforming in space yields

$$\delta B_y^R/\delta B_y^I = -\cot(\omega_- t),$$
$$\delta B_y^R/\delta B_y^R = -\cot(\omega_- t), \tag{23}$$

so that

$$\theta = \theta_R = \omega_- t - \pi/2. \tag{24}$$

As time increases then, both θ and θ_R should increase, the first meaning forward propagation and the second left-circular polarization. This is indeed what is observed in Figs. 3a and b. Furthermore, the measured period is of the order of the Alfven period as predicted by theory.

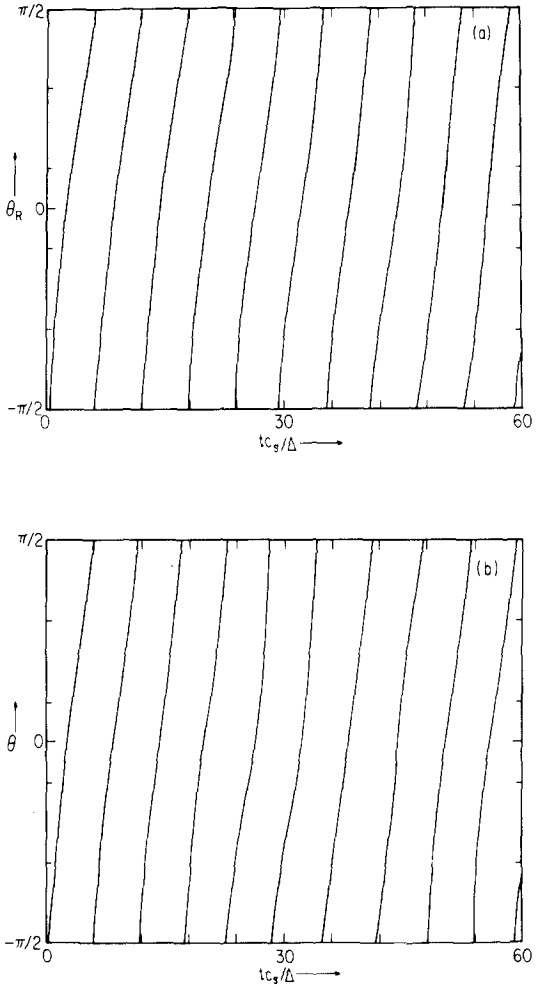

FIG. 3. Phase diagnostics: left-circularly polarized forward propagating launched wave with wavenumber $k = (2\pi/L_x)m$, $m = 2$. (a) The temporal behavior of the simulation angle $\theta_R = \tan^{-1}(\delta B_y^R/\delta B_z^R)$. (b) The time evolution of the simulation angle $\theta = \tan^{-1}(\delta B_y^R/\delta B_y^I)$.

These results show that the one-fluid code with addition of the Hall term correctly propagates Alfven-ion cyclotron waves and whistler waves.

IV. Conclusions

A particle algorithm for performing computer simulations of collective plasma behaviors in the magnetohydrodynamic regime has been developed. It presents an extension of our previous particle magnetohydrodynamic codes; it only requires the addition of the Hall term, and yet enriches the physics by describing some of the electron dynamics without resorting to a two-fluid code. The algorithm is based on the approximations of a massless electron equation, quasi-neutrality, and negligible displacement current for the electron–ion fluid description of plasmas. This algorithm has been successfully implemented with full nonlinear dynamics. We verified that the code allows both the Alfven-ion cyclotron waves and the whistler waves through dispersion relation, propagation and polarization checks. This code should have a variety of applications to the study of plasma phenomena for frequencies of the order of the ion gyrofrequency with almost the same computation speed and core requirement as the one-fluid magnetohydrodynamic code. This code dispenses with the information of the velocity distributions; however, it would not be difficult to retain such features, since the code is based on particle methods and a fixed grid system. Such an algorithm, in general, would enrich the conventional Eulerian magnetohydrodynamic codes as well.

Appendix

For stability of the code, we primarily discuss the parallel propagating Alfven waves (whistler and ion-cyclotron waves). The magnetosonic waves in the perpendicular direction are unaffected by addition of the Hall term. In the low β plasma, the sound frequency is much smaller than the Alfvèn frequency, so that we neglect pressure effects in the stability analysis. The equation of interest is essentially

$$\mathbf{B}^{n+1} = \langle \mathbf{B} \rangle^n + \Delta t\, \nabla \times (\mathbf{v} \times \mathbf{B})^n + \Delta t\, \nabla \times [\tilde{\alpha} \mathbf{B} \times (\nabla \times \mathbf{B})]^n,$$

where the angular bracket denotes spatial averaging required to stabilize the Lax algorithm and the superscripts denote the time step.

The finite difference equation for magnetic fields may be schematically written after linearization as [6, 7]

$$\begin{aligned} B^{n+1}_{yl,j} = {} & \tfrac{1}{4}(B^n_{yl+1,j} + B^n_{yl-1,j} + B^n_{yl,j+1} + B^n_{yl,j-1}) \\ & - \frac{\Delta t}{2\Delta} v_x (B^n_{yl+1,j} - B^n_{yl-1,j}) - \frac{\Delta t}{2\Delta} v_y (B^n_{yl,j+1} - B^n_{yl,j-1}) \\ & + \tilde{\alpha} \frac{\Delta t}{\Delta^2} B_0 (B^n_{zl+1,j} - 2B^n_{zl,j} + B^n_{z,l-1,j}), \end{aligned} \tag{A1}$$

$$B_{zi,j}^{n+1} = \tfrac{1}{4}(B_{zi+1,j}^{n} + B_{zi,j+1}^{n} + B_{zi,j+1}^{n} + B_{zi,j-1}^{n})$$
$$- \frac{\Delta t}{2\Delta} v_x (B_{zi+1,j}^{n} - B_{zi-1,j}^{n}) - \frac{\Delta t}{2\Delta} v_y (B_{zi,j+1}^{n} - B_{zi,j-1}^{n})$$
$$- \tilde{\alpha} \frac{\Delta_t}{\Delta^2} B_0 (B_{yi+1,j}^{n} - 2B_{yi,j}^{n} + B_{yi-1,j}^{n}), \tag{A2}$$

where subscripts i and j indicate the grid coordinates. Here, we are concerned with the Alfven wave propagating along the x-axis parallel to the external magnetic field $\mathbf{B}_0$. We therefore neglected B_x. By assuming that $B_{i,j}^{n}$ goes like $\exp[-in\omega\,\Delta t + i(k_x i\Delta + k_y j\Delta)]$, we obtain

$$gB_y = [\tfrac{1}{2}(\cos\alpha + \cos\beta) - i\theta_x \Delta t \sin\alpha - i\theta_y \Delta t \sin\beta] B_y + 2\frac{\tilde{\alpha} B_0 \Delta t}{\Delta^2}(\cos\alpha - 1) B_z, \tag{A3}$$

$$gB_z = [\tfrac{1}{2}(\cos\alpha + \cos\beta) - i\theta_x \Delta t \sin\alpha - i\theta_y \Delta t \sin\beta] B_z - 2\frac{\tilde{\alpha} B_0 \Delta t}{\Delta^2}(\cos\alpha - 1) B_y, \tag{A4}$$

where $g = e^{-i\omega\Delta t}$, $\alpha = k_x \Delta$, $\beta = k_y \Delta$, $\theta_x = v_x/\Delta$, and $\theta_y = v_y/\Delta$.

The value of g is determined by the determinant of the above matrix equation:

$$0 = \det \begin{vmatrix} g - [\tfrac{1}{2}(\cos\alpha + \cos\beta) - i\theta_x \Delta t \sin\alpha - i\theta_y \Delta t \sin\beta], & -\dfrac{2\tilde{\alpha} B_0 \Delta t}{\Delta^2}(\cos\alpha - 1) \\ \dfrac{2\tilde{\alpha} B_0 \Delta t}{\Delta^2}(\cos\alpha - 1), & g - [\tfrac{1}{2}(\cos\alpha + \cos\beta) - i\theta_x \Delta t \sin\alpha - i\theta_y \Delta t \sin\beta] \end{vmatrix}. \tag{A5}$$

If we set $\tilde{\alpha} = 0$ (no Hall term), we obtain conventional stability criterion [6] for the Lax algorithm by demanding $|g| \leqslant 1$:

$$\Delta t \leqslant \frac{3^{1/2}\Delta}{(v_x^2 + v_y^2)^{1/2} 2} = \frac{3^{1/2}\Delta}{(v_A^2 + c_s^2)^{1/2} 2}. \tag{A6}$$

Let us now consider the Hall term effect on the code stability in the Lax algorithm. For simplicity, we drop the term involving θ_x and θ_y. Then, the amplification factor g from Eq. (A5) is

$$g = \tfrac{1}{2}(\cos\alpha + \cos\beta) \pm \frac{i\tilde{\alpha} 2 B_0 \Delta t}{\Delta^2}(\cos\alpha - 1). \tag{A7}$$

The stability condition for the code is

$$|g| \leqslant 1 \tag{A8}$$

for all wavenumbers. This reads

$$F[q=\cos(k_x\Delta)] = \tfrac{1}{4}[\cos(k_x\Delta)+\cos(k_y\Delta)]^2 + \frac{4\tilde{\alpha}^2 B_0^2 \Delta t^2}{\Delta^4}[1-\cos(k_x\Delta)]^2 - 1 \leqslant 0. \tag{A9}$$

For the parallel propagating Alfven wave, $F(q)$ in Eq. (A9) is zero at $q=\cos(k_x\Delta)=1$ and $F(q)$ is concave $[F''(q)>0]$ over the period $0\leqslant q\leqslant 1$. The necessary and sufficient condition for stability, therefore, becomes $F(q=0)\leqslant 0$. This leads to the stability criterion for the Lax algorithm with the Hall term

$$\Delta t \leqslant \frac{3^{1/2}}{4}\frac{\Delta^2}{\tilde{\alpha}B_0} = \frac{3^{1/2}}{4}\frac{\Delta^2}{v_A^2/\Omega_i}, \tag{A10}$$

where $q=0$ is taken at $k_x\Delta=\pi/2$. In general, the stability is determined by the more stringent of the two [Eqs. (A6) and (A10)]. In our case, Eq. (A6) gives $\Delta t\leqslant 0.21$ and Eq. (A10) demands $\Delta t\leqslant 0.16$ with $v_A=3c_s$ and $\Omega_i=3\,c_s/\Delta$; we have, therefore, the theoretical limit $\Delta t\leqslant 0.16$. The code in our simulation runs is stable at $\Delta t=0.15$ and unstable at $t=0.2$, in reasonable agreement with the present analysis.

In order to analyze the finite size effects we derive the dispersion relation from Eqs. (A1) and (A2). In a manner similar to that for deriving Eq. (A5), we obtain

$$0=\det\begin{vmatrix} -i\omega-\frac{1}{2}(\cos\alpha-1)-\frac{1}{2}(\cos\beta-1)+i\theta_x\Delta t\sin\alpha+i\theta_y\Delta t\sin\beta, & \dfrac{2\tilde{\alpha}B_0\Delta t}{\Delta^2}(\cos\beta-1) \\ \dfrac{-2\tilde{\alpha}B_0\Delta t}{\Delta^2}(\cos\alpha-1), & i\omega-\frac{1}{2}(\cos\alpha-1)-\frac{1}{2}(\cos\beta-1)+i\theta_x\Delta t\sin\alpha+i\theta_y\Delta t\sin\beta \end{vmatrix}. \tag{A11}$$

Here we have put $B_{i,j}^{n+1}-B_{i,j}^n=-i\omega B_{i,j}^n$. A quadratic equation, Eq. (A11), may be solved as

$$\omega=\theta_x\Delta t\sin\alpha+\theta_y\Delta t\sin\beta\pm\frac{2\tilde{\alpha}B_0\Delta t}{\Delta^2}(1-\cos\alpha) - i\tfrac{1}{2}[(1-\cos\alpha)+(1-\cos\beta)]. \tag{A12}$$

For example, the e^{-1} damping time of a longest wave in a 64 grid system is $400\,\Delta/c_s$. The first two terms give the Alfven disperion at small wavenumbers as $k_x v_A$ (or $k_y c_A$). The third term originates from the Hall term and yields the frequency splitting into the whistler and ion-cyclotron waves. Note that since we neglected the pressure effect in the low β plasma, the compressional effect is absent in Eq. (A12). The last term is purely imaginary and is a damping term due to the finite differencing.

Let us consider the first term. As the wavenumber k_x increases, the linear dispersion $k_x v_A$ bends over and approaches a finite number as k_x approaches the Brillouin zone ($k_x=k_{BZ}\equiv\pi/2\Delta$). This is a typical Brillouin effect. Moreover, we

have the effect of the third term. For the upper branch (whistler wave), the bending effect due to the third term is in the complementary direction, while for the lower branch (ion-cyclotron wave), it adds up. It is, however, noted that the Hall term should give rise to a frequency splitting proportional to k_x^2 in a "continuous" plasma in the small wavenumber regime. The finite differencing of the Hall term gives this feature correctly at $k_x \ll k_{BZ}$, but the frequency splitting becomes proportional to k_x as k_x increases away from $k_x = 0$ towards $k_x \lesssim k_{BZ}$. Thus, the linear tendency of the frequency split $\Delta\omega(k_x)$ in larger wavelengths is the finite differencing effect on the Hall effect in the code. Also note that these modes with heavy dispersive or Brillouin effects suffer strong damping because of the fourth term in Eq. (A12), which helps alleviate the unphysical dispersion that comes into play in physics runs of the code.

Finally, let us discuss numerical effects on the pressure term. The pressure term is calculated with the Fast Fourier Transform algorithm [5]. From the equation of motion, the sound wave equations for an isothermal plasma are

$$\rho \frac{d}{dt}\mathbf{v} = -\int dr' f(r-r')\,\nabla' P(r') \tag{A13}$$

and

$$P(r) = T\int dr' f(r-r')\,n(r'), \tag{A14}$$

where T is the plasma temperature. In Fourier space Eqs. (A13) and (A14) read

$$-i\omega v = ic_s^2 k f(k)^2\, n(k) \tag{A15}$$

after linearization, where c_s is the sound speed and $f(k)$ is the form factor $\exp(-k^2a^2/2)$ for a Gaussian-shaped particle with a size a. With the help of the continuity equation, we obtain the dispersion relation for the sound wave as

$$\omega^2 = k^2 c_s^2 \exp(-k^2a^2). \tag{A16}$$

If $a \sim \Delta$, which is a conventional choice, the numerical dispersion arising from the finite-sized particle effect is of the same order of magnitude and character as those due to the finite differencing discussed above: both tend to bend the linear dispersion over in the neighborhood of the Brillouin zone boundary.

ACKNOWLEDGMENTS

This work was supported by the National Science Foundation under Grants PHY 76-83686 and ATM 78-19253.

REFERENCES

1. H. OKUDA, J. M. DAWSON, A. T. LIN, AND C. C. LIN, *Phys. Fluids* **21** (1978), 476.
2. D. W. HEWETT AND C. W. NIELSON, *J. Comput. Phys.* **29** (1978), 219.
3. J. A. BYERS, B. I. COHEN, W. C. CONDIT, AND J. D. HANSEN, *J. Comput. Phys.* **27** (1978), 363.
4. K. V. ROBERTS AND D. E. POTTER, "Methods in Computational Physics," Vol. 9, p. 339, Academic Press, New York, 1976.
5. J. N. LEBOEUF, T. TAJIMA, AND J. M. DAWSON, *J. Comput. Phys.* **31** (1979), 379.
7. D. E. POTTER, "Computational Physics," Chap. III, Wiley, New York, 1973.
7. R. D. RICHTMEYER AND K. W. MORTON, "Difference Methods for Initial-Value Problems," p. 360, Wiley, New York, 1967.